Nano-Hexapod - Test Bench

Dehaeze Thomas

October 29, 2024

Contents

In the previous section, all the struts were mounted and individually characterized. Now the nano-hexapod is assembled using a mounting procedure described in Section 1.

In order to identify the dynamics of the nano-hexapod, a special suspended table is developed which consists of a stiff "optical breadboard" suspended on top of four soft springs. The Nano-Hexapod is then fixed on top of the suspended table, such that its dynamics is not affected by complex dynamics except from the suspension modes of the table that can be well characterized and modelled (Section 2).

The obtained nano-hexapod dynamics is analyzed in Section 3, and compared with the Simscape model in Section 4.

1 Nano-Hexapod Assembly Procedure

The assembly of the nano-hexapod is quite critical to both avoid additional stress in the flexible joints (that would result in a loss of stroke) and for the precise determination of the Jacobian matrix. The goal is to fix the six struts to the two nano-hexapod plates (shown in Figure 1.1a) while the two plates are parallel, aligned vertically, and such that all the flexible joints do not experience any stress. Do to so, a precisely machined mounting tool (Figure 1.1b) is used to position the two nano-hexapod plates during the assembly procedure.
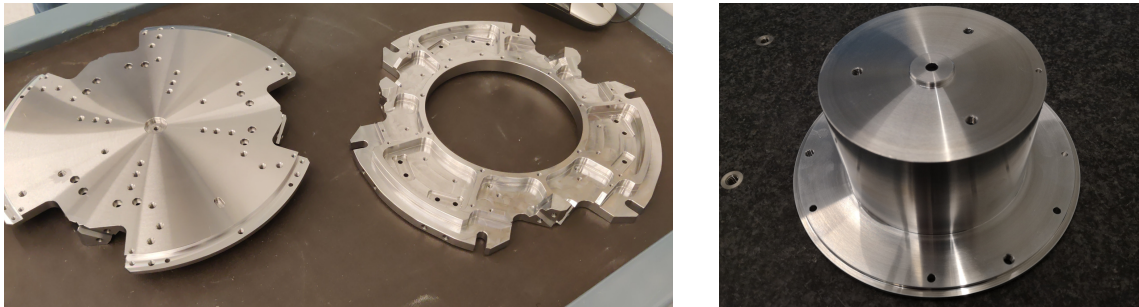
(a) Received top and bottom plates

(b) Mounting tool

Figure 1.1: Received Nano-Hexapod plates (a) and mounting tool used to position the two plates during assembly (b)

The mechanical tolerances of the received plates are checked using a FARO arm[1] (Figure 1.2a) and are found to comply with the requirements[2]. The same is done for the mounting tool[3] The two plates are then fixed to the mounting tool as shown in Figure 1.2b. The main goal of this "mounting tool" is to position the flexible joint interfaces (the "V" shapes) of both plates such that a cylinder can rest on the 4 flat interfaces at the same time.

The quality of the positioning can be estimated by measuring the "straightness" of the top and bottom "V" interfaces. This corresponds to the diameter of the smallest cylinder that contains all points of the measured axis. This is again done using the FARO arm, and the results for all the six struts are summarized in Table 1.1. The straightness is found to be better than $15\,\mu m$ for all the struts[4], which is sufficiently good to not induce significant stress of the flexible joint during the assembly.

The encoder rulers and heads are then fixed to the top and bottom plates respectively (Figure 1.3). The encoder heads are then aligned to maximize the received contrast.

The six struts are then fixed to the bottom and top plates one by one. First the top flexible joint is

---

[1]Faro Arm Platinum 4ft, specified accuracy of $\pm 13\mu m$

[2]Location of all the interface surfaces with the flexible joints are checked. The fits (182H7 and 24H8) with the interface element are checked.

[3]The height dimension is better than $40\,\mu m$. The diameter fit of 182g6 and 24g6 with the two plates is verified.

[4]As the accuracy of the FARO arm is $\pm 13\,\mu m$, the true straightness is probably better than the values indicated. The limitation of the instrument is here reached.
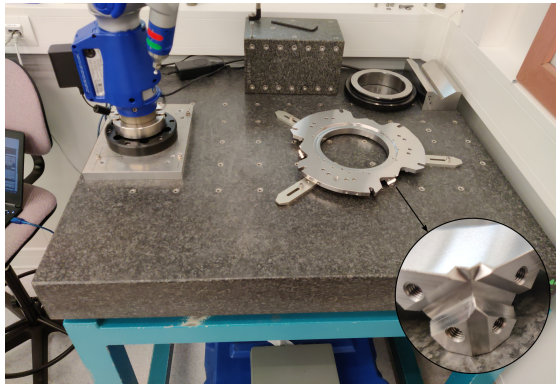
(a) Dimensional check of the bottom plate
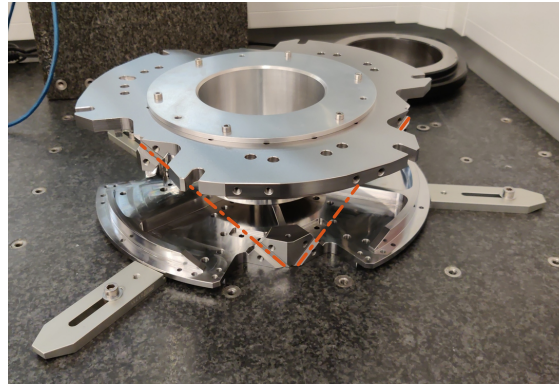
**(b)** Wanted coaxiality between interfaces

Figure 1.2: A Faro arm is used to dimensionally check the received parts (a) and after mounting the two plates with the mounting part (b)

Strut	Meas 1	Meas 2
1	$7\,\mu m$	$3\,\mu m$
2	$11\,\mu m$	$11\,\mu m$
3	$15\,\mu m$	$14\,\mu m$
4	$6\,\mu m$	$6\,\mu m$
5	$7\,\mu m$	$5\,\mu m$
6	$6\,\mu m$	$7\,\mu m$

Table 1.1: Measured straightness between the two "V" for the six struts. These measurements are performed two times for each strut.

(a) Encoder rulers
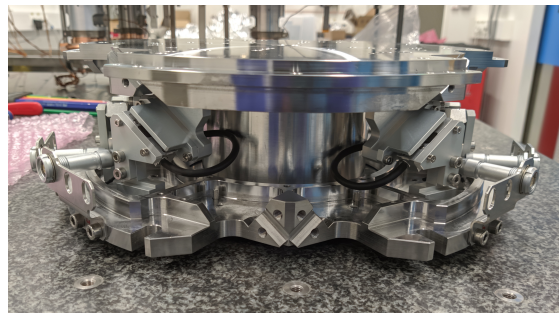
(b) Encoder heads

Figure 1.3: Mounting of the encoders to the Nano-hexapod. The rulers are fixed to the top plate (a) while the encoders heads are fixed to the botom plate (b)

fixed such that its flat reference surface is in contact with the top plate. This is to precisely known the position of the flexible joint with respect to the top plate. Then the bottom flexible joint is fixed. After all six struts are mounted, the mounting tool (Figure 1.1b) can be disassembled, and the fully mounted nano-hexapod as shown in Figure 1.4 is obtained.
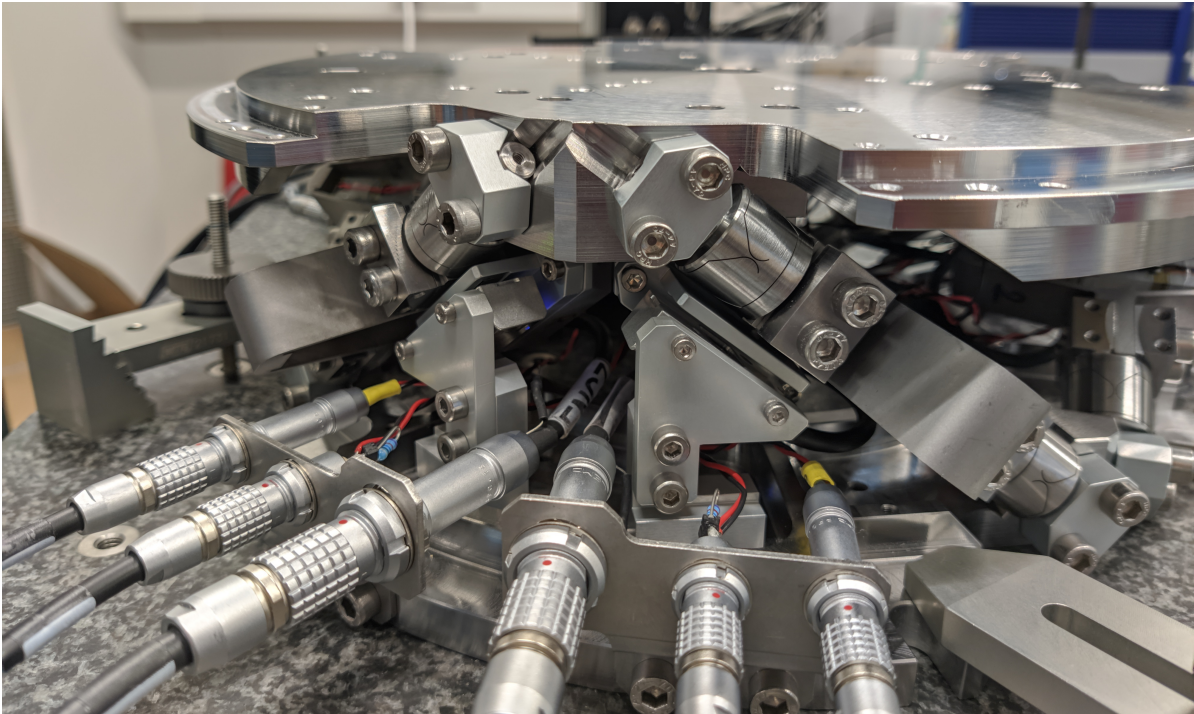
Figure 1.4: Mounted Nano-Hexapod

2 Suspended Table

## 2.1 Introduction

When a dynamical system is fixed to a support (such as a granite or an optical table), its dynamics will couple to the support dynamics. This may results in additional modes appearing in the system dynamics, which are difficult to predict and model. Two prevent this issue, strategy adopted here is to mount the nano-hexapod on top a suspended table with low frequency suspension modes.

In such a case, the modes of the suspended table are chosen to be at much lower frequency than those of the nano-hexapod such that they are well decoupled. An other key advantage is that the suspension modes of the suspended table can be easily modelled using Simscape. Therefore, the measured dynamics of the nano-hexapod on top of the suspended table can be compared to a simscape model representing the same experimental conditions. The model of the Nano-Hexapod can thus be precisely tuned to match the measured dynamics.

The developed suspended table is presented in Section 2.2. The modal analysis of the table is done in 2.3. Finally, the Simscape model representing the suspended table is tuned to match the measured modes (Section 2.4).

2.2 Experimental Setup

The design of the suspended table is quite straightforward. First, an optical table with high frequency flexible mode was selected[1]. Then, four springs[2] were selected with low enough spring rate such that the suspension modes are below 10Hz. Finally, some interface elements were designed, and mechanical lateral mechanical stops were added (Figure 2.1).
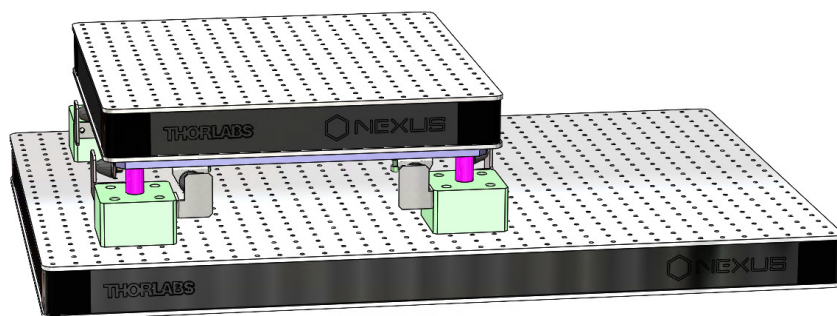
**Figure 2.1:** CAD View of the vibration table. Purple cylinders are representing the soft springs.

---

[1] The 450 mm x 450 mm x 60 mm Nexus B4545A from Thorlabs.
[2] "SZ8005 20 x 044" from Steinel. The spring rate is specified at $17.8\,N/mm$

2.3 Modal analysis of the suspended table

In order to perform a modal analysis of the suspended table, a total of 15 3-axis accelerometers[3] were fixed to the breadboard. Using an instrumented hammer, the first 9 modes could be identified and are summarized in Table 2.1. The first 6 modes are suspension modes (i.e. rigid body mode of the breadboard) and are located below 10Hz. The next modes are flexible modes of the breadboard as shown in Figure 2.3, and located above 700Hz.
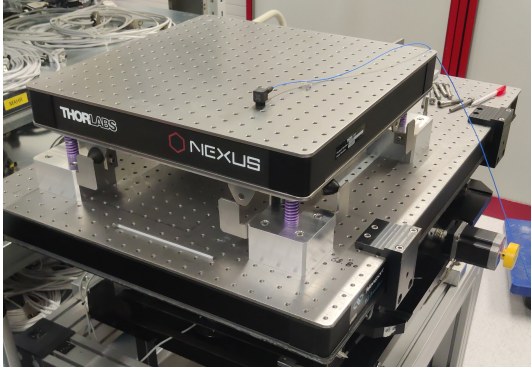
Figure 2.2: Mounted suspended table. Only 1 or the 15 accelerometer is mounted on top

Modes	Frequency	Description
1,2	1.3 Hz	X-Y translations
3	2.0 Hz	Z rotation
4	6.9 Hz	Z translation
5,6	9.5 Hz	X-Y rotations
7	701 Hz	"Membrane" Mode
8	989 Hz	Complex mode
9	1025 Hz	Complex mode

Table 2.1: Obtained modes of the suspended table

(a) Flexible mode at 701Hz

(b) Flexible mode at 989Hz



(c) Flexible mode at 1025Hz
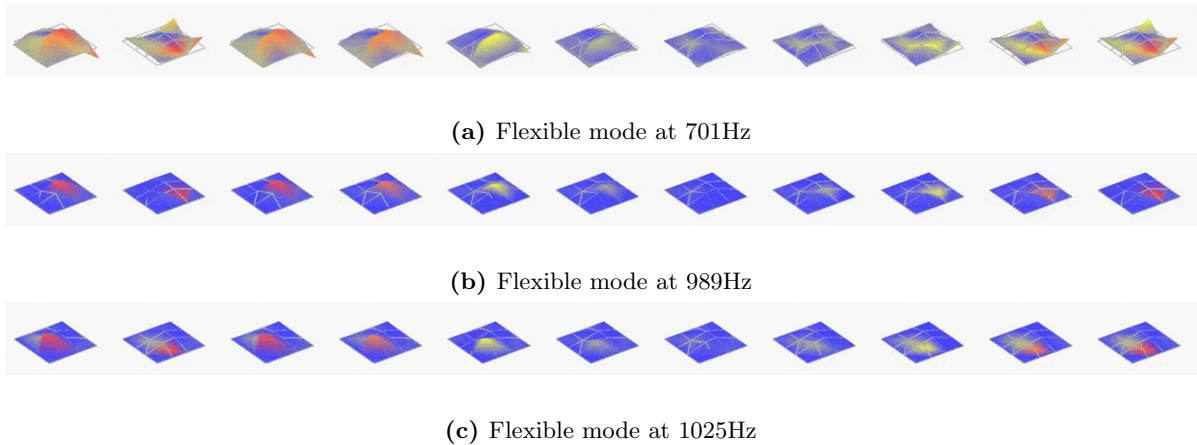
Figure 2.3: Three identified flexible modes of the suspended table

2.4 Simscape Model of the suspended table

The Simscape model of the suspended table simply consists of two solid bodies connected by 4 springs. The 4 springs are here modelled with "bushing joints" that have stiffness and damping properties in x, y and z directions. The 3D representation of the model is displayed in Figure 2.4 where the 4 "bushing joints" are represented by the blue cylinders.

---

[3]PCB 356B18. Sensitivity is $1\,V/g$, measurement range is $\pm 5\,g$ and bandwidth is 0.5 to 5 kHz.
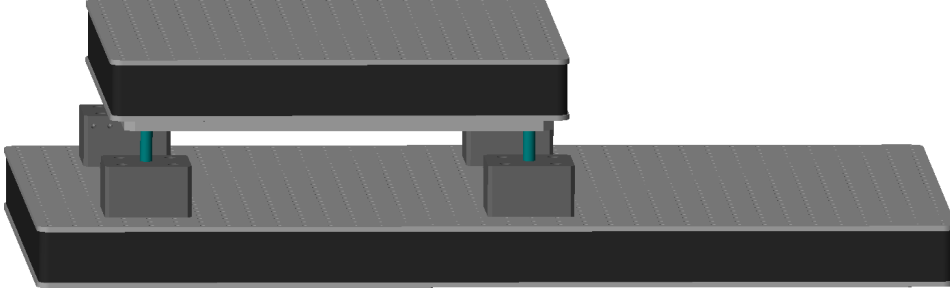
Figure 2.4: 3D representation of the simscape model

The model order is 12, and it represents the 6 suspension modes. The inertia properties of the parts are set from the geometry and material densities. The stiffness of the springs was initially set from the datasheet nominal value of $17.8\,N/mm$ and then reduced down to $14\,N/mm$ to better match the measured suspension modes. The stiffness of the springs in the horizontal plane is set at $0.5\,N/mm$. The obtained suspension modes of the simscape model are compared with the measured ones in Table 2.2.

Directions	D_x, D_y	R_z	D_z	R_x, R_y
Experimental	1.3 Hz	2.0 Hz	6.9 Hz	9.5 Hz
Simscape	1.3 Hz	1.8 Hz	6.8 Hz	9.5 Hz

Table 2.2: Comparison of the identified suspension modes with the Simscape model and measured experimentally

Conclusion

In this section, a suspended table with low frequency suspension modes and high frequency flexible modes was presented. This suspended table will be used in Section 3 for dynamical identification of the Nano-Hexapod. The objective is to be able to accurately identify the dynamics of the nano-hexapod, isolated from complex support dynamics. The key point of this strategy is to be able to accurately model the suspended table.

To do so, a modal analysis of the suspended table was performed in Section 2.3, validating the low frequency suspension modes and high frequency flexible modes. Then, a multi-body model of this suspended table was tuned to match with the measurements (Section 2.4).

3 Nano-Hexapod Measured Dynamics

The Nano-Hexapod is then mounted on top of the suspended table as shown in Figure 3.1. All the instrumentation (Speedgoat with ADC, DAC, piezoelectric voltage amplifiers and digital interfaces for the encoder) are setup and connected to the nano-hexapod using many cables.
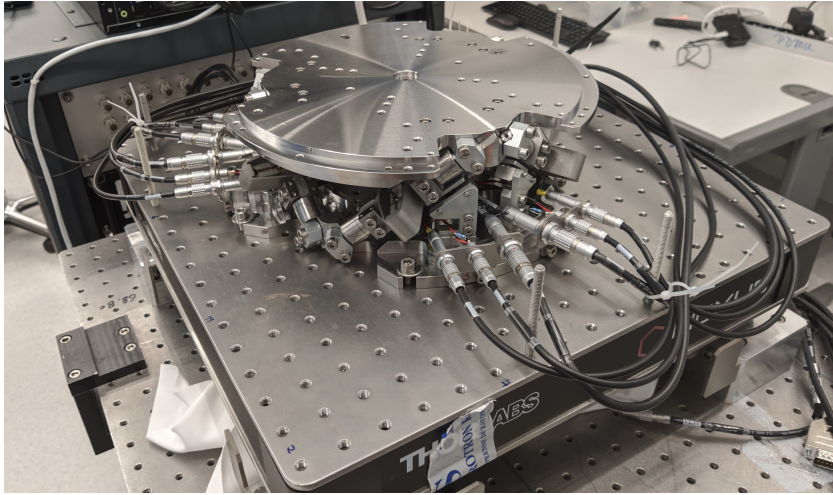
Figure 3.1: Mounted Nano-Hexapod on top of the suspended table

A modal analysis of the nano-hexapod is first performed in Section 3.1. It will be used to better understand the measured dynamics from actuators to sensors.

A block diagram schematic of the (open-loop) system is shown in Figure 3.2. The transfer function from controlled signals $\mathbf{u}$ to the force sensors voltages $\mathbf{V}_s$ and to the encoders measured displacements $\mathbf{d}_e$ are identified in Section 3.2. The effect of the payload mass on the dynamics is studied in Section 3.3.
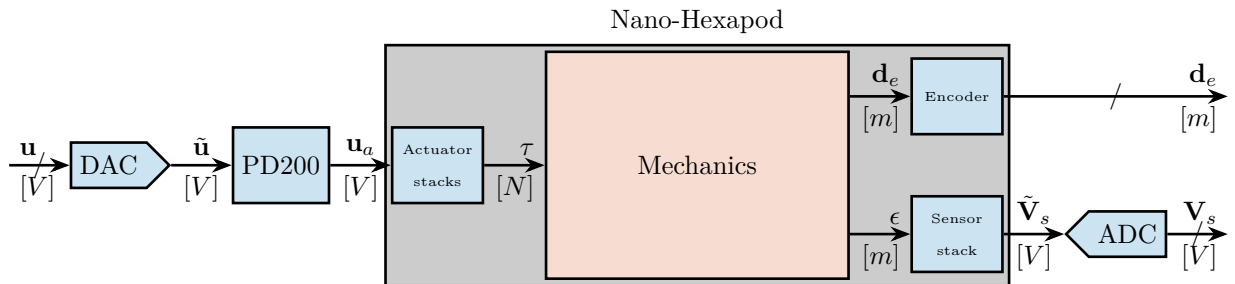
Figure 3.2: Block diagram of the system. Command signal generated by the speedgoat is $\mathbf{u}$, the measured dignals are $\mathbf{d}_e$ and $\mathbf{V}_s$. Units are indicated in square brackets.

3.1 Modal analysis

In order to ease the future analysis of the measured plant dynamics, a basic modal analysis of the nano-hexapod is performed. Five 3-axis accelerometers are fixed on the top platform of the nano-hexapod (Figure 3.3) and the top platform is excited using an instrumented hammer.
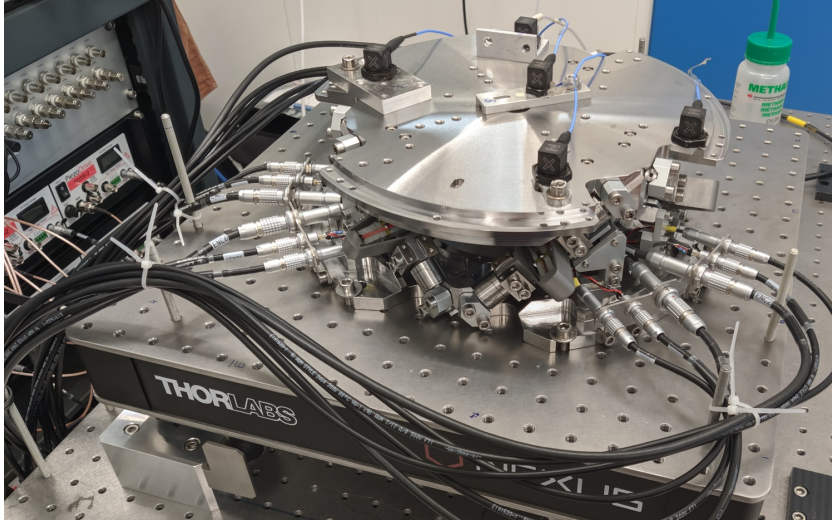
Figure 3.3: Five accelerometers fixed on top of the nano-hexapod to perform a modal analysis

Between 100Hz and 200Hz, 6 suspension modes (i.e. rigid body modes of the top platform) are identified. At around 700Hz, two flexible modes of the top plate are observed (see Figure 3.4). These modes are summarized in Table 3.1.

Mode	Frequency	Description
1	120 Hz	Suspension Mode: Y-translation
2	120 Hz	Suspension Mode: X-translation
3	145 Hz	Suspension Mode: Z-translation
4	165 Hz	Suspension Mode: Y-rotation
5	165 Hz	Suspension Mode: X-rotation
6	190 Hz	Suspension Mode: Z-rotation
7	692 Hz	(flexible) Membrane mode of the top platform
8	709 Hz	Second flexible mode of the top platform

Table 3.1: Description of the identified modes of the Nano-Hexapod

3.2 Identification of the dynamics

The dynamics of the nano-hexapod from the six command signals (u_1 to u_6) the six measured displacement by the encoders (d_{e1} to d_{e6}) and to the six force sensors (V_{s1} to V_{s6}) are identified by generating a low pass filtered white noise for each of the command signals, one by one.

The 6×6 FRF matrix from $\mathbf{u}$ ot $\mathbf{d}_e$ is shown in Figure 3.5. The diagonal terms are displayed using colorful lines, and all the 30 off-diagonal terms are displayed by grey lines.

(a) Flexible mode at 692Hz


(b) Flexible mode at 709Hz
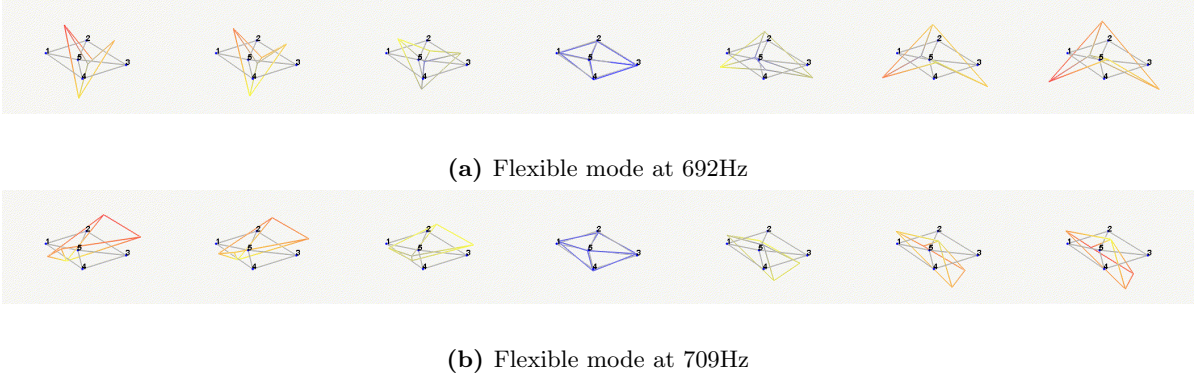
Figure 3.4: Two identified flexible modes of the top plate of the Nano-Hexapod

All the six diagonal terms are well superimposed up to at least $1\,kHz$, indicating good manufacturing and mounting uniformity. Below the first suspension mode, good decoupling can be observed (the amplitude of the all of off-diagonal terms are ≈ 20 times smaller than the diagonal terms).

From 10Hz up to 1kHz, around 10 resonance frequencies can be observed. The first 4 are suspension modes (at 122Hz, 143Hz, 165Hz and 191Hz) which correlate the modes measured during the modal analysis in Section 3.1. Then, three modes at 237Hz, 349Hz and 395Hz are attributed to the internal strut resonances (this will be checked in Section 4.2). Except the mode at 237Hz, their amplitude is rather low. Two modes at 665Hz and 695Hz are attributed to the flexible modes of the top platform. Other modes can be observed above 1kHz, which can be attributed to flexible modes of the encoder supports or to flexible modes of the top platform.

Up to at least 1kHz, an alternating pole/zero pattern is observed, which renders the control easier to tune. This would not have been the case if the encoders were fixed to the struts.
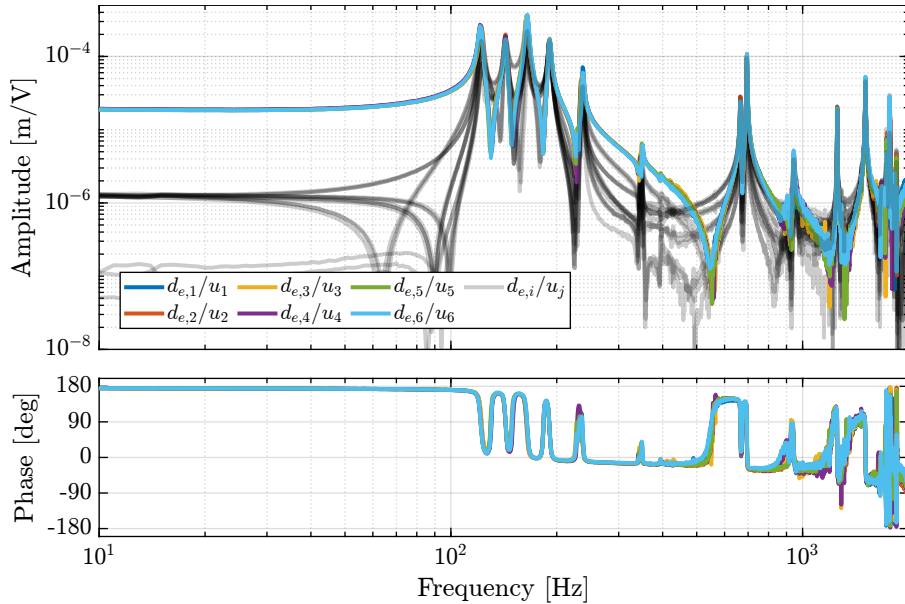
Figure 3.5: Measured FRF for the transfer function from $\mathbf{u}$ to $\mathbf{d}_e$. The 6 diagonal terms are the colorfull lines (all superimposed), and the 30 off-diagonal terms are the shaded black lines.

Similarly, the 6×6 FRF matrix from $\mathbf{u}$ to $\mathbf{V}_s$ is shown in Figure 3.6. Alternating poles and zeros is observed up to at least 2kHz, which is a necessary characteristics in order to apply decentralized IFF. Similar to what was observed for the encoder outputs, all the "diagonal" terms are well superimposed, indicating that the same controller can be applied for all the struts. The first flexible mode of the struts as 235Hz is appearing, and therefore is should be possible to add some damping to this mode using IFF.
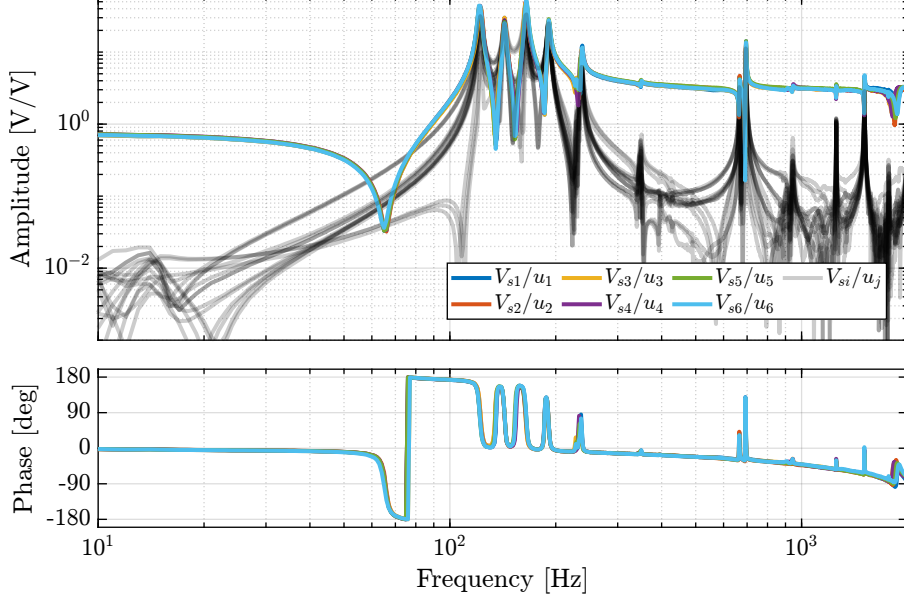
Figure 3.6: Measured FRF for the transfer function from $\mathbf{u}$ to $\mathbf{V}_s$. The 6 diagonal terms are the colorfull lines (all superimposed), and the 30 off-diagonal terms are the shaded black lines.

3.3 Effect of payload mass on the dynamics

As one major challenge in the control of the NASS is the wanted robustness to change of payload mass, it is necessary to understand how the dynamics of the nano-hexapod changes with a change of payload mass.

In order to study this change of dynamics with the payload mass, up to three "cylindrical masses" of $13\,kg$ each can be added for a total of $\approx 40\,kg$. These three cylindrical masses on top of the nano-hexapod are shown in Figure 3.7.

The identified dynamics are then saved for further use. The obtained frequency response functions from actuator signal u_i to the associated encoder d_{ei} for the four payload conditions (no mass, 13kg, 26kg and 39kg) are shown in Figure 3.8a. As expected, the frequency of the suspension modes are decreasing with an increase of the payload mass. The low frequency gain does not change as it is linked to the stiffness property of the nano-hexapod, and not to its mass property.

The frequencies of the two flexible modes of the top plate are first decreased a lot when the first mass is added (from $\approx 700\,Hz$ to $\approx 400\,Hz$). This is due to the fact that the added mass is composed of two half cylinders which are not fixed together. It therefore adds a lot of mass to the top plate without adding stiffness in one direction. When more than one "mass layer" is added, the half cylinders are added with some angles such that rigidity are added in all directions (see how the three mass "layers"
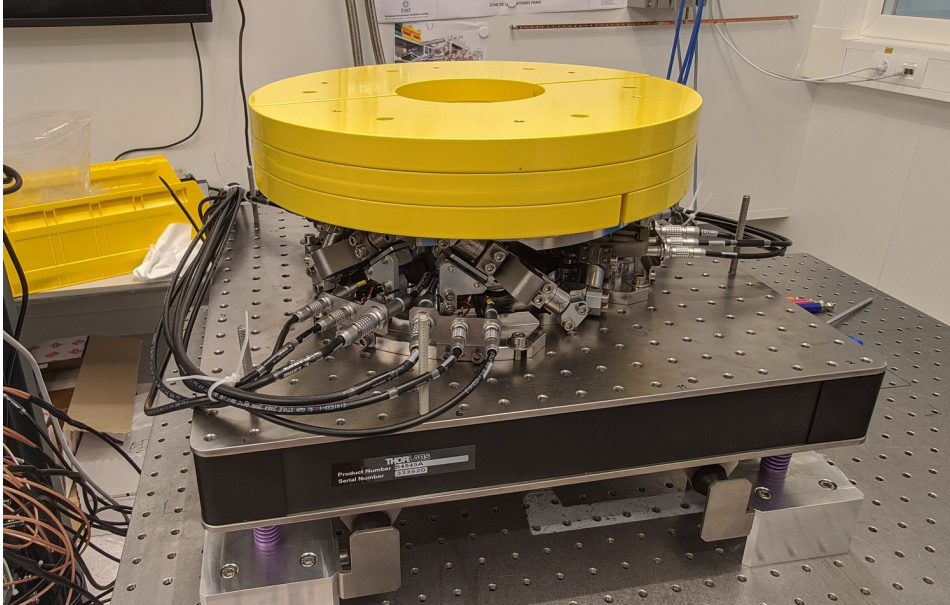
Figure 3.7: Picture of the nano-hexapod with the added three cylindrical masses for a total of $\approx 40\,kg$

are positioned in Figure 3.7). In that case, the frequency of these flexible modes are increased. In practice, the payload should be one solid body, and no decrease of the frequency of this flexible mode should be observed. The apparent amplitude of the flexible mode of the strut at 237Hz becomes smaller as the payload mass is increased.
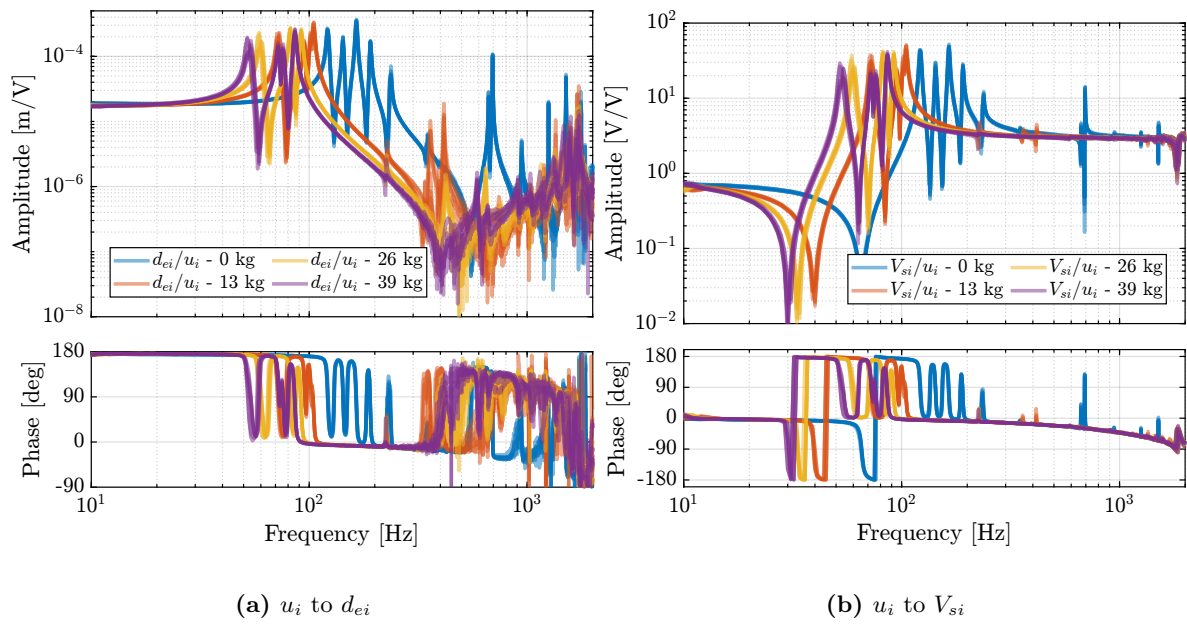
The measured FRF from u_i to V_{si} are shown in Figure 3.8b. For all the tested payloads, the measured FRF always have alternating poles and zeros, indicating that IFF can be applied in a robust way.

Conclusion

After the Nano-Hexapod was fixed on top of the suspended table, its dynamics was identified.

The frequency response functions from the six DAC voltages $\mathbf{u}$ to the six encoders measured displacements $\mathbf{d}_e$ displays alternating complex conjugate poles and complex conjugate zeros up to at least 1kHz. At low frequency, the coupling is small, indicating correct assembly of all parts. This should enables the design of a decentralized positioning controller based on the encoder for relative positioning purposes. The suspension modes and flexible modes measured during the modal analysis (Section 3.1) are also observed in the dynamics. Lot's of other modes are present above 700Hz, which will inevitably limit the achievable bandwidth. The observed effect of the payload's mass on the dynamics is quite large, which also represent a complex control challenge.

The frequency response functions from the six DAC voltages $\mathbf{u}$ to the six force sensors voltages $\mathbf{V}_s$ all have alternating complex conjugate poles and complex conjugate zeros. This indicates that it should be possible to implement decentralized Integral Force Feedback in a robust way. This alternating property holds for all the tested payloads.

(a) u_i to d_{ei}

(b) u_i to V_{si}

Figure 3.8: Measured Frequency Response Functions from u_i to d_{ei} (a) and from u_i to V_{si} (b) for all 4 payload conditions. Only diagonal terms are shown.

4 Nano-Hexapod Model Dynamics

In this section, the measured dynamics done in Section 3 is compared with the dynamics estimated from the Simscape model. The nano-hexapod simscape model is therefore added on top of the vibration table Simscape model as shown in Figure 4.1.
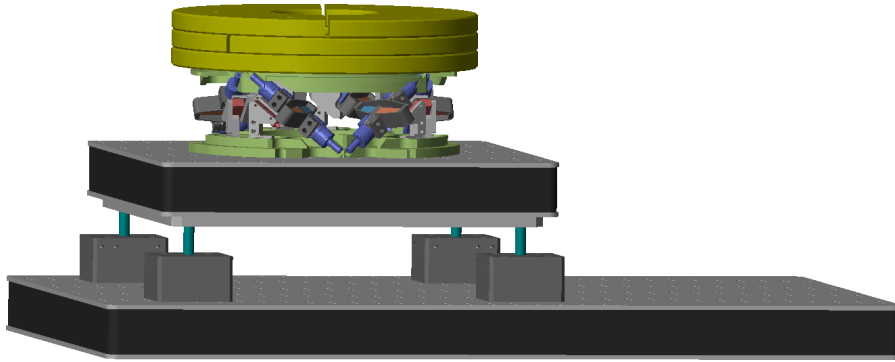
Figure 4.1: 3D representation of the simscape model with the nano-hexapod on top of the suspended table. Three mass "layers" are here added

The model should exhibit certain characteristics that are verified in this section. First, it should match the measured system dynamics from actuators to sensors that were presented in Section 3. Both the "direct" terms (Section 4.1) and "coupling" terms (Section 4.2) of the Simscape model are compared with the measured dynamics. Second, it should also represents how the system dynamics changes when a payload is fixed to the top platform. This is checked in Section 4.3.

4.1 Nano-Hexapod model dynamics

The Simscape model of the nano-hexapod is first configured with 4-DoF flexible joints, 2-DoF APA and rigid top and bottom platforms. The stiffness of the flexible joints are chosen based on the values estimated using the test bench and based on FEM. The parameters of the APA model are the ones determined from the test bench of the APA. The 6×6 transfer function matrices from $\mathbf{u}$ to $\mathbf{d}_e$ and from $\mathbf{u}$ to $\mathbf{V}_s$ are extracted then from the Simscape model.

A first feature that should be checked is that the model well represents the "direct" terms of the measured FRF matrix. To do so, the diagonal terms of the extracted transfer function matrices are compared with the measured FRF in Figure 4.2. It can be seen that the 4 suspension modes of the nano-hexapod (at 122Hz, 143Hz, 165Hz and 191Hz) are well modelled. The three resonances that were attributed to "internal" flexible modes of the struts (at 237Hz, 349Hz and 395Hz) cannot be seen in the model, which is reasonable as the APA are here modelled as a simple uniaxial 2-DoF system. At higher

frequencies, no resonances can be seen in the model, as the as the top plate and the encoder supports are modelled as rigid bodies.

(a) from u to d_e
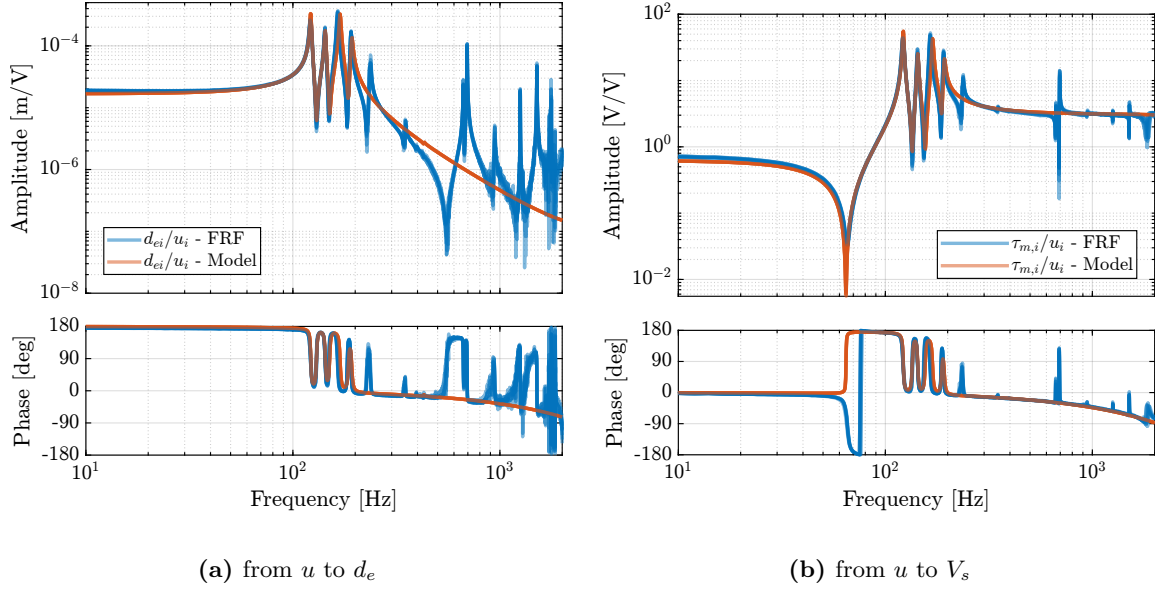
(b) from u to V_s

Figure 4.2: Comparison of the diagonal elements (i.e. "direct" terms) of the measured FRF matrix and the identified dynamics from the Simscape model. Both for the dynamics from u to d_e (a) and from u to V_s (b)

4.2 Modelling dynamical coupling

Another wanted feature of the model is that it well represents the coupling in the system as this is often the limiting factor for the control of MIMO systems. Instead of comparing the full 36 elements of the 6×6 FFR matrix from $\mathbf{u}$ to $\mathbf{d}_e$, only the first "column" is compared (Figure 4.3), which corresponds to the transfer function from the command u_1 to the six measured encoder displacements d_{e1} to d_{e6}. It can be seen that the coupling in the model is well matching the measurements up to the first un-modelled flexible mode at 237Hz. Similar results are observed for all the other coupling terms, as well as for the transfer function from $\mathbf{u}$ to $\mathbf{V}_s$.

The APA300ML are then modelled with a *super-element* extracted from a FE-software. The obtained transfer functions from u_1 to the six measured encoder displacements d_{e1} to d_{e6} are compared with the measured FRF in Figure 4.4. While the damping of the suspension modes for the *super-element* is underestimated (which could be solved by properly tuning the proportional damping coefficients), the flexible modes of the struts at 237Hz and 349Hz are well modelled. Even the mode 395Hz can be observed in the model. Therefore, if the modes of the struts are to be modelled, the *super-element* of the APA300ML may be used, at the cost of obtaining a much higher order model.

4.3 Modelling the effect of payload mass

Another important characteristics of the model is that it should well represents the dynamics of the system for all considered payloads. The model dynamics is therefore compared with the measured
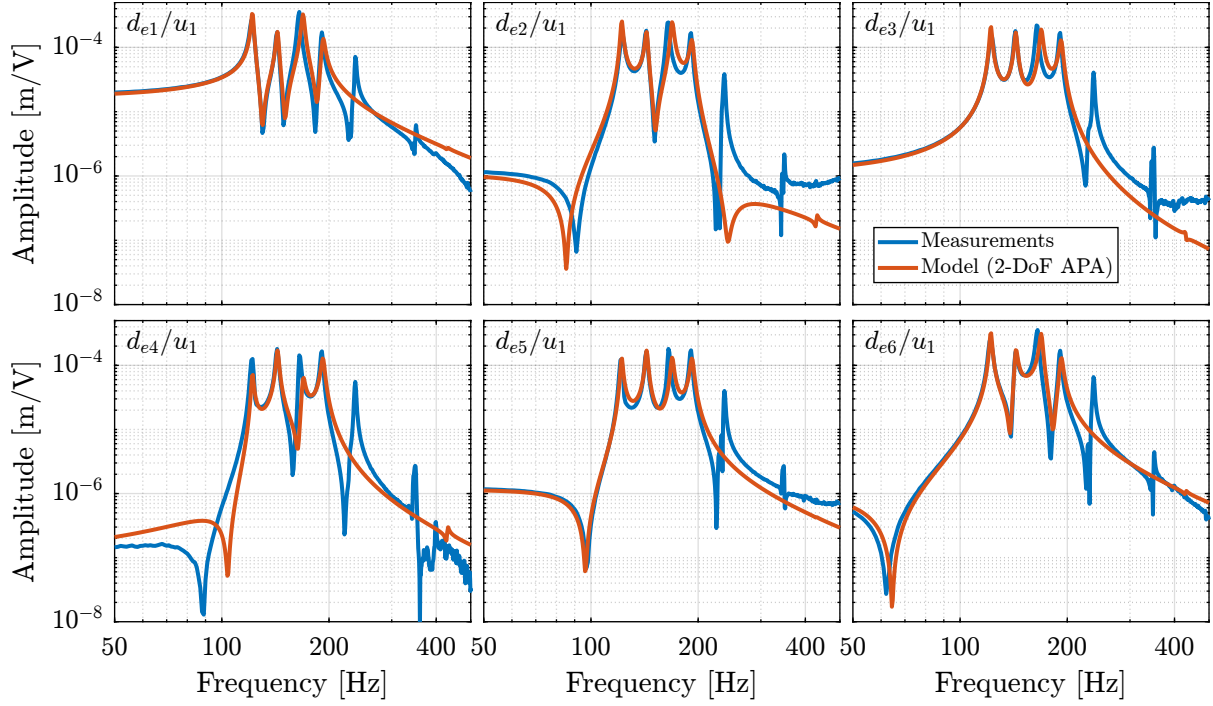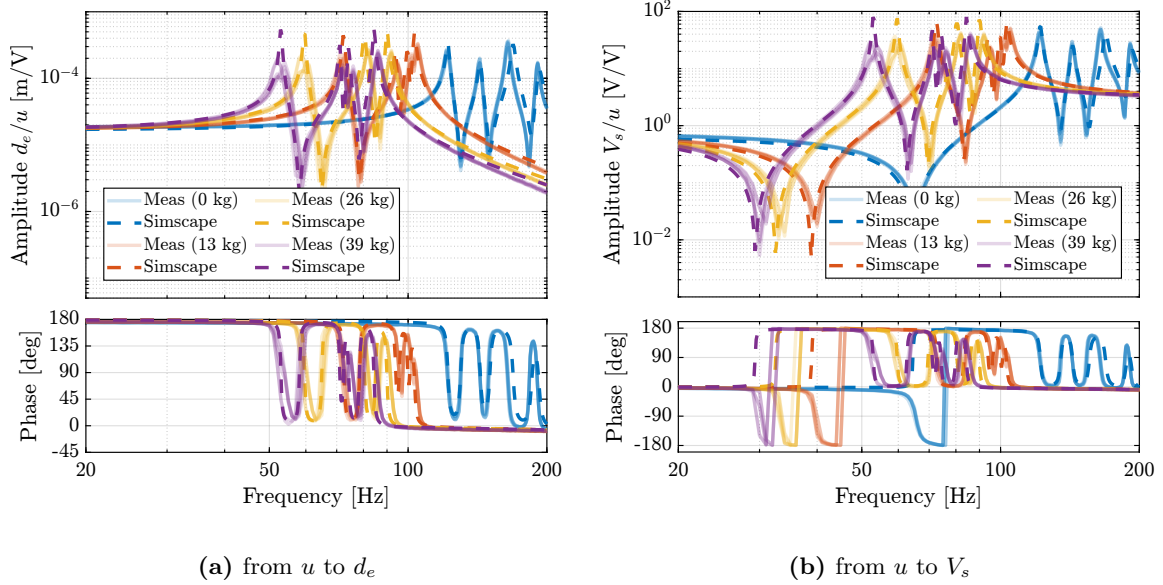
Figure 4.3: Comparison of the measured (in blue) and modelled (in red) frequency transfer functions from the first control signal u_1 to the six encoders d_{e1} to d_{e6}
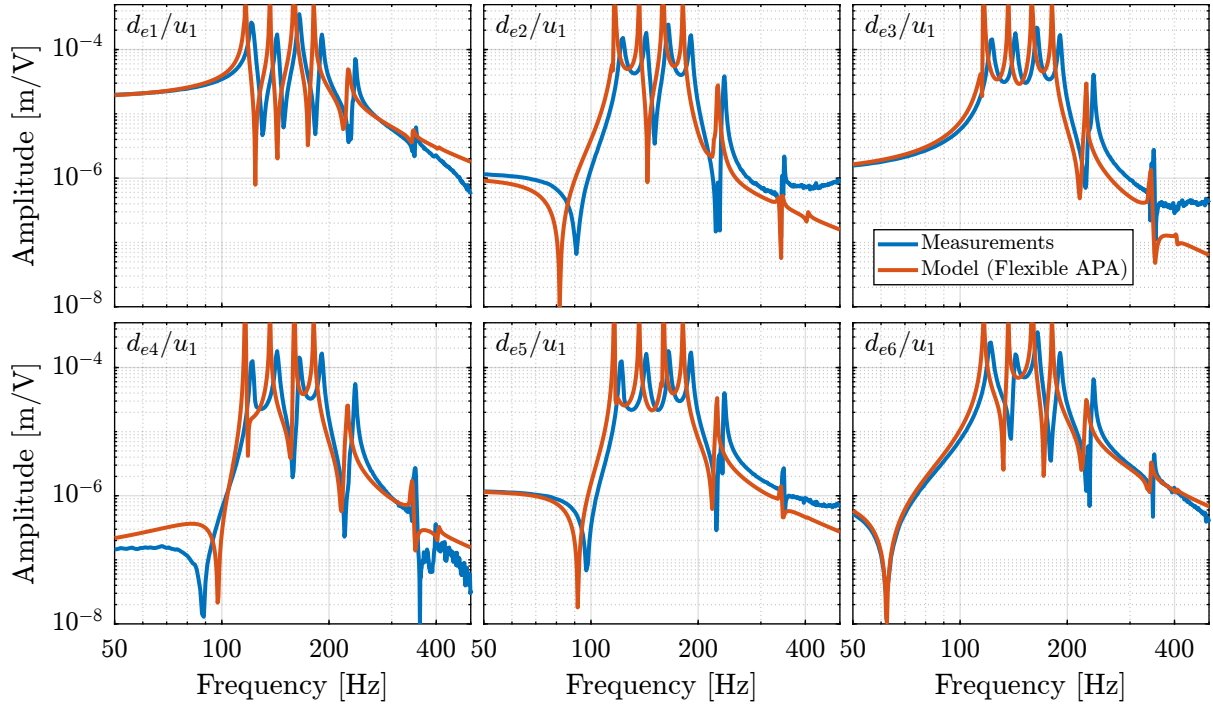
Figure 4.4: Comparison of the measured (in blue) and modelled (in red) frequency transfer functions from the first control signal u_1 to the six encoders d_{e1} to d_{e6}

dynamics for 4 payloads (no payload, 13kg, 26kg and 39kg) in Figure 4.5. The observed shift to lower frequency of the suspension modes with an increased payload mass is well represented by the Simscape model. The complex conjugate zeros are also well matching with the experiments both for the encoder outputs (Figure 4.5a) and the force sensor outputs (Figure 4.5b).

Note that the model displays smaller damping that what is observed experimentally for high values of the payload mass. One option could be to tune the damping as a function of the mass (similar to what is done with the Rayleigh damping). However, as decentralized IFF will be applied, the damping will be brought actively, and the open-loop damping value should have very little impact on the obtained plant.


(a) from u to d_e

(b) from u to V_s

Figure 4.5: Comparison of the diagonal elements (i.e. "direct" terms) of the measured FRF matrix and the identified dynamics from the Simscape model. Both for the dynamics from u to d_e (a) and from u to V_s (b)

In order to also check if the model well represents the coupling when high payload masses are used, the transfer functions from u_1 to d_{e1} to d_{e6} are compared in the case of the 39kg payload in Figure 4.6. Excellent match between the experimental coupling and the model coupling is observed. The model therefore well represents the system dynamical coupling for different considered payloads.

Conclusion

As illustrated in this section, the developed Simscape model accurately represents the suspension modes of the Nano-Hexapod. Both FRF matrices from $\mathbf{u}$ to $\mathbf{V}_s$ and from $\mathbf{u}$ to $\mathbf{d}_e$ are well matching with the measurements, even when considering coupling (i.e. off-diagonal) terms, which are very important from a control perspective.

At frequency above the suspension modes, the Nano-Hexapod model becomes inaccurate as the flexible modes are not modelled. It was shown that modelling the APA300ML using a "super-element" allows to model the internal resonances of the struts. The same could be done with the top platform and the
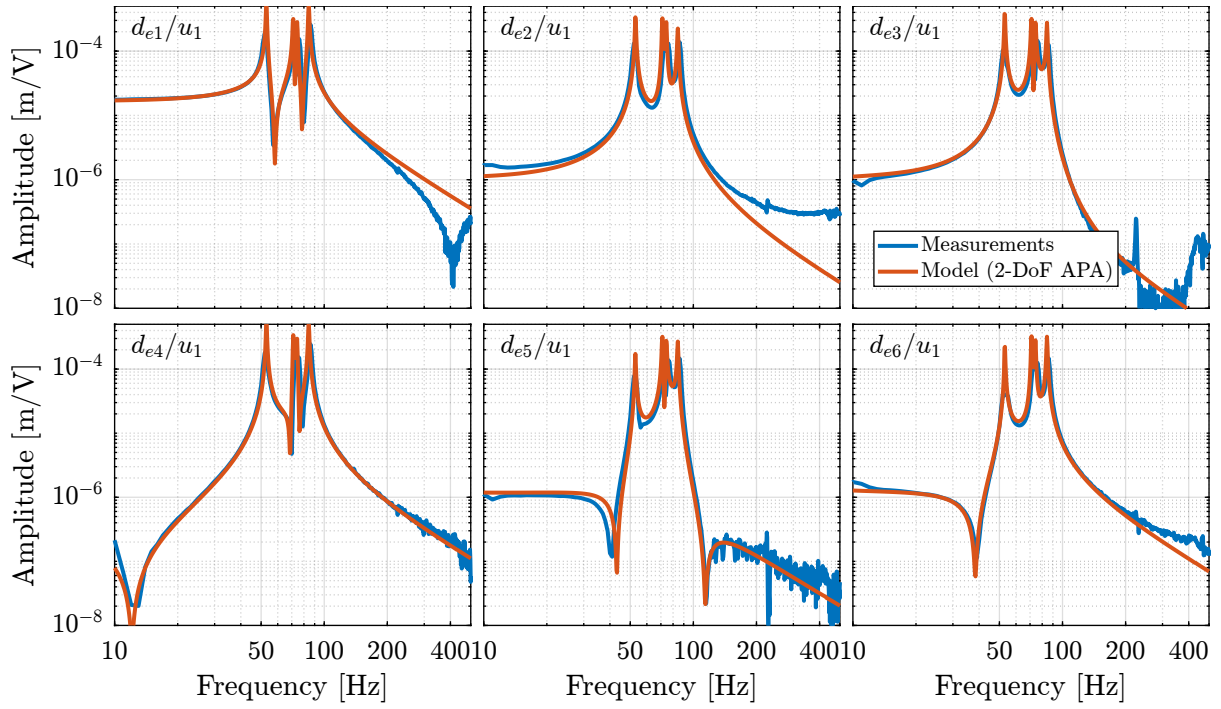
Figure 4.6: Comparison of the measured (in blue) and modelled (in red) frequency transfer functions from the first control signal u_1 to the six encoders d_{e1} to d_{e6}

encoder supports, but the model order would be higher and may become unpractical for simulation purposes.

5 Conclusion

The goal of this test bench was to obtain an accurate model of the nano-hexapod that can then be included on top of the micro-station model.

This strategy was to measure the nano-hexapod in conditions where all factors that could have impacted the nano-hexapod dynamics were taken into account. This was done by developing a suspended table with low frequency suspension modes which can be accurately modelled.

While the dynamics of the nano-hexapod was indeed impacted by the dynamics of the suspended platform, this impact was also taken into account in the Simscape model, and a good match was obtained.

Obtaining a model accurately representing the complex dynamics of the Nano-Hexapod was made possible by the modelling approach used during this work. This approach consisted of tuning and validating models of individual components (such as the APA and flexible joints) using dedicated test benches. Only then, the different models could be combined to form the Nano-Hexapod dynamical model. If a model of the nano-hexapod was developed in one time, it would be difficult to tune all model parameters to match the measured dynamics, or even to know if the model "structure" would be adequate to represents the system dynamics.

Bibliography

[1] S. Skogestad and I. Postlethwaite, *Multivariable Feedback Control: Analysis and Design - Second Edition*. John Wiley, 2007.

[2] M. Indri and R. Oboe, *Mechatronics and Robotics: New Trends and Challenges*. CRC Press, 2020.